# *Edge-localized mode avoidance and pedestal structure in I-mode plasmas*



**Citation:** Walk, J. R., J. W. Hughes, A. E. Hubbard, J. L. Terry, D. G. Whyte, A. E. White, S. G. Baek, et al. "Edge-Localized Mode Avoidance and Pedestal Structure in I-Mode Plasmas." Phys. Plasmas 21, no. 5 (May 2014): 056103.

**As Published:** http://dx.doi.org/10.1063/1.4872220

**Publisher:** American Institute of Physics (AIP)

**Persistent URL:** http://hdl.handle.net/1721.1/95894

**Version:** Original manuscript: author's manuscript prior to formal peer review

PSFC/JA-13-45

# ELM Avoidance and Pedestal Structure in I-Mode Plasmas

Walk, J.R.; Hughes, J.W.; Snyder, P.B.*; Hubbard, A.E.; Terry, J.L.; Dominguez, A.**; Osborne, T.*; Cziegler, I.***; Whyte, D.G.; Baek, S.G.; Reinke, M.L.; Theiler, C.; Churchill, R.M.; Rice, J.E.

* General Atomics
** Princeton Plasma Physics Laboratory
*** UCSD Center for Momentum Transport and Flow Organization

December, 2013

**Plasma Science and Fusion Center**
**Massachusetts Institute of Technology**
**Cambridge MA 02139 USA**

This work was supported by the U.S. Department of Energy, Grant No. DE-FC02-99ER54512. Theory work at General Atomics was supported by the U.S. Department of Energy, Grant no. DE-FG02-99ER54309. 

Accepted for publication to *Physics of Plasmas.*

# ELM Avoidance and Pedestal Structure in I-Mode Plasmas

JR Walk,* JW Hughes, AE Hubbard, JL Terry, DG Whyte, AE White, SG Baek, ML Reinke, C Theiler, RM Churchill, and JE Rice

*MIT Plasma Science and Fusion Center*

PB Snyder and T Osborne

*General Atomics*

A Dominguez

*Princeton Plasma Physics Laboratory*

I Cziegler

*UCSD Center for Momentum Transport and Flow Organization*

(Dated: January 22, 2014)

I-mode is a high-performance tokamak regime characterized by the formation of a temperature pedestal and enhanced energy confinement, without an accompanying density pedestal or drop in particle and impurity transport. I-mode operation appears to have naturally-occurring suppression of large ELMs in addition to its highly favorable scalings of pedestal structure and overall performance. Extensive study of the ELMy H-mode has led to the development of the EPED model, which utilizes calculations of coupled peeling-ballooning MHD modes and kinetic-ballooning mode (KBM) stability limits to predict the pedestal structure preceding an ELM crash. We apply similar tools to the structure and ELM stability of I-mode pedestals. Analysis of I-mode discharges prepared with high-resolution pedestal data from the most recent C-Mod campaign reveals favorable pedestal scalings for extrapolation to large machines – pedestal temperature scales strongly with power per particle $P_{net}/\overline{n}_e$, and likewise pedestal pressure scales as the net heating power (consistent with weak degradation of confinement with heating power). Matched discharges in current, field, and shaping demonstrate the decoupling of energy and particle transport in I-mode, increasing fueling to span nearly a factor of two in density while maintaining matched temperature pedestals with consistent levels of $P_{net}/\overline{n}_e$. This is consistent

with targets for increased performance in I-mode, elevating pedestal $\beta_p$ and global performance with matched increases in density and heating power. MHD calculations using the ELITE code indicate that I-mode pedestals are strongly stable to edge peeling-ballooning instabilities. Likewise, numerical modeling of the KBM turbulence onset, as well as scalings of the pedestal width with poloidal beta, indicate that I-mode pedestals are not limited by KBM turbulence – both features identified with the trigger for large ELMs, consistent with the observed suppression of large ELMs in I-mode.

PACS numbers: 52.55.Fa, 52.55.Tn, 52.35.Py, 52.25.Fi, 52.40.Hf

* jrwalk@psfc.mit.edu

## I. INTRODUCTION

Concepts for the development of tokamak magnetic-confinement fusion into an economical form of power generation are characterized by two overarching requirements. First, a high level of energy confinement is necessary for net energy production and the desired level of self-heating of the plasma by fusion products. At the same time, particle transport must be sufficient to avoid the deleterious effects of accumulated helium "ash" and other impurities on fusion performance. A number of operating regimes, collectively referred to as "high-confinement" or H-modes, satisfying these requirements has been established, the most successful of which is the ELMy H-mode [1], which is therefore considered the baseline for operation on ITER [2, 3].

H-modes are characterized by a steep gradient region in density, temperature, and pressure at the plasma edge – the *pedestal* – the height of which strongly correlates with overall performance [4]. However, this introduces an additional constraint – the steep gradients found in the pedestal region have been shown to drive Edge-Localized Mode (ELM) MHD instabilities [5–7]. While bursty ELM transport regulates impurity confinement in ELMy H-mode, on ITER-scale devices ELM heat pulses lead to unacceptable levels of erosion and damage to plasma-facing materials [8, 9]. As such, recent efforts have focused on mitigating or avoiding large ELMs in high-performance regimes, either via engineering solutions (e.g., pellet pacing [10] or resonant magnetic perturbations [11–14]) or via alternate high-performance scenarios which inherently avoid large ELMs, e.g. the EDA H-mode [15, 16] or QH Mode [17–19].

The I-mode [20, 21], explored on the Alcator C-Mod tokamak [22], is such an alternative regime to H-mode operation. I-mode is unique among high-performance regimes in that it appears to decouple energy and particle transport, attaining the desired H-mode levels of energy confinement while maintaining L-mode levels of particle transport, naturally achieving the desired flushing of impurities from the plasma. This manifests in the edge of the plasma by the formation of a steep temperature pedestal without the accompanying density pedestal found in conventional H-modes (see Figure 1), and with the formation of an edge $E_r$ well comparable to that found in H-mode [21, 23, 24]. I-mode also appears to be naturally stable against large ELMs, avoiding the need for active ELM control systems. Finally, energy confinement in I-mode shows little to no degradation with input heating power [20],

in contrast to the degradation of confinement in ELMy H-mode (roughly $\tau_E \sim P^{-0.7}$ from multi-machine analyses [2]) – a potentially highly-favorable scaling to reactor-scale devices.

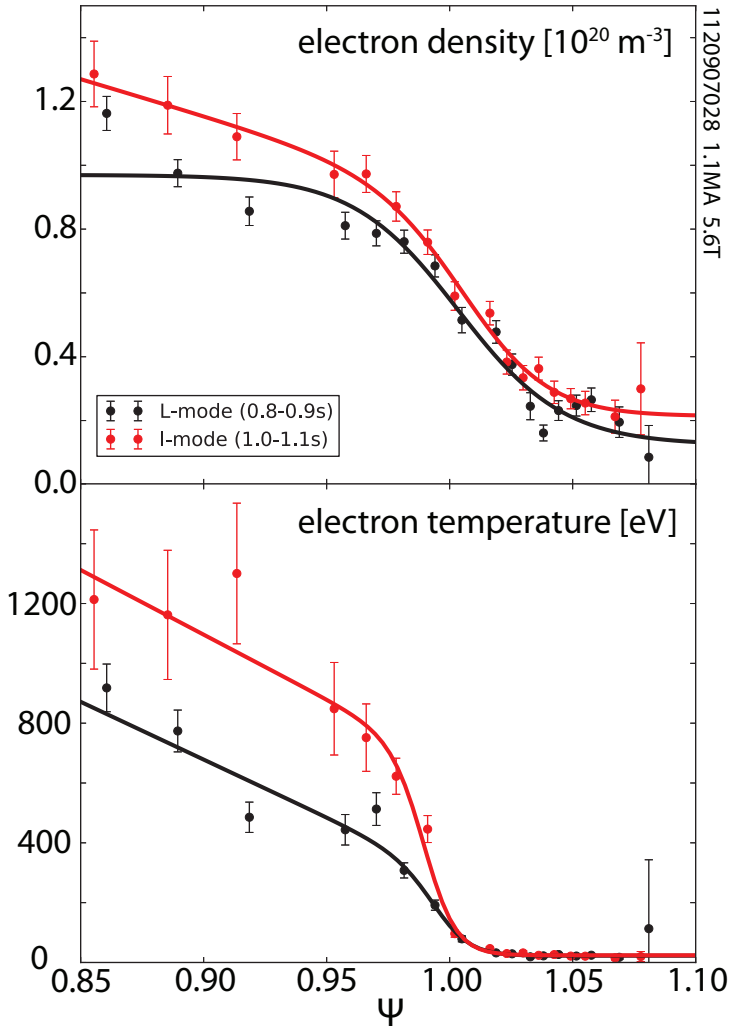


FIG. 1. Example $n_e$ and $T_e$ edge profiles, comparing L-mode (black) and I-mode (red) from a single discharge. I-mode maintains a comparable edge density, without the formation of a steep gradient region, while forming an H-mode-like temperature pedestal.

A firm understanding of the pedestal is essential for the extrapolation of any high-performance regime to ITER and reactor-scale devices: the pedestal structure sets a strong constraint on overall performance [4], as well as determining stability against large, deleterious ELMs. Recent cooperative efforts among theory, modeling, and experiment [25] have resulted in a predictive model, termed EPED [26–28], for ELMy H-mode based on coupled constraints from peeling-ballooning MHD stability [29–31] and kinetic-ballooning turbulence

[32]. The EPED model has successfully predicted pedestal structure in ELMy H-mode on a number of machines [25, 33, 34] spanning a range of parameters, reaching ITER-relevant pedestal pressures in the case of H-modes on Alcator C-Mod. We apply a similar approach to the study of I-mode pedestals. First, we explore the empirical scalings of I-mode pedestals, which is important for extrapolation to larger machines and can give an intuitive picture of pedestal MHD stability (section III). Second, we take a detailed computational approach to the MHD stability of I-mode pedestals (section IV). Finally, we examine the turbulence characteristics of the I-mode pedestal region, notably the observed Weakly-Coherent Mode (WCM) fluctuation found in I-mode (section V).

## II. I-MODE ACCESS AND EXPERIMENTAL SETUP

I-mode experiments were carried out on the Alcator C-Mod tokamak [22], a compact, high-field device with major radius $R \sim 0.67$ m, minor radius $a \sim 0.22$ m, and toroidal magnetic field $B_T \leq 8.1$ T. Alcator C-Mod operates with entirely high-$Z$ metal plasma-facing components, and reaches comparable divertor heat flux to that anticipated for ITER [35–37]. High-performance operation is commonly assisted by boronization treatment of plasma-facing materials – however, a recent boronization is not typically necessary in I-mode due to the low particle confinement. Alcator C-Mod plasmas are heated with up to 5.5 MW of ion-cyclotron RF power.

I-mode operation is robustly accessible on Alcator C-Mod, with steady I-modes sustained in a variety of shapes and edge current profiles, and with low to moderate collisionality (see Figure 2). Notably, I-mode operation is naturally near ITER targets for edge collisionality and safety factor. Here we use for the collisionality

$$\nu^* = 6.921 \times 10^{-18} \frac{R q n_e Z_{eff} \ln \Lambda_e}{\varepsilon^{3/2} T_e^2} \tag{1}$$

with electron density $n_e$ in m$^{-3}$ and temperature $T_e$ in eV, major radius $R$ in m, and with the Coulomb logarithm defined by $\ln \Lambda_e = 24 - \ln\left(\sqrt{n_e}/T_e\right)$. For pedestal collisionality, $\nu^*_{95}$, we evaluate $n_e$, $T_e$, and safety factor $q$ at the 95% flux surface. I-mode operation has been maintained with heating power up to $\sim 2\times$ the L-I transition threshold without entering H-mode [38, 39] (see Figure 3).

I-mode is typically accessed in the "unfavorable" drift configuration – that is, with ion

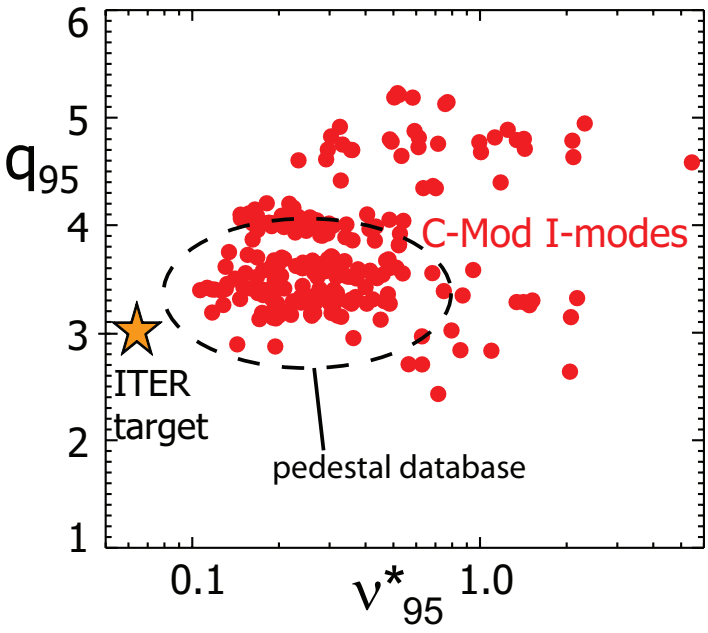


FIG. 2. Edge collisionality and safety factors with accessible I-modes, with ITER target for comparison. Data from the high-resolution pedestal database are highlighted.

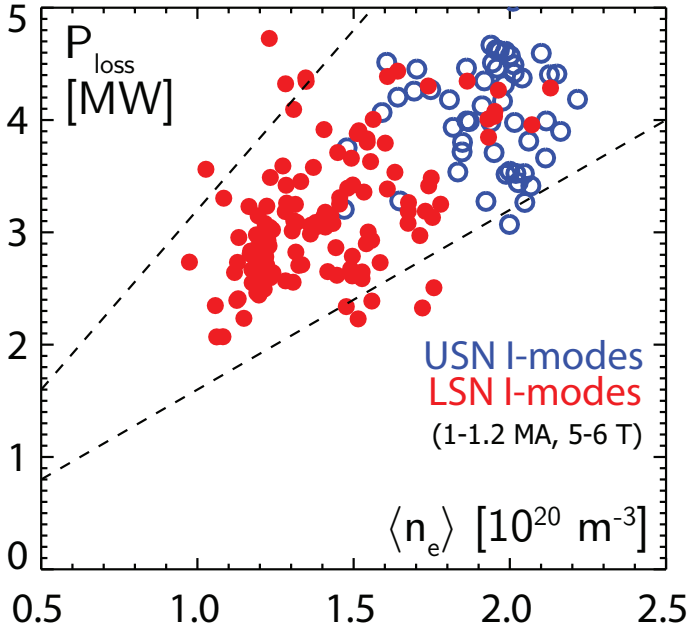


FIG. 3. Example line-averaged density and power range ($P_{loss} = P_{ICRF} + P_{Ohm} - dW/dt$) of USN and LSN I-mode access, illustrating $\sim 2 \times P_{thres}$ access range for 1-1.2 MA, 5-6 T I-modes. USN shapes are forward-field and LSN shapes are reversed-field, such that all I-modes shown are in the unfavorable drift configuration.

$\nabla B$ drift directed away from the primary X-point [20]. This elevates the H-mode threshold power [40], widening the range over which I-mode can be sustained. This drift configuration has been achieved both with standard field and current in an upper-null shape, and in a lower-null shape with reversed field and current. I-mode experiments in the most recent run campaign have focused on reversed-field LSN plasmas, which exhibit the widest access window and avoid difficulties with pedestal diagnostics. A subset of the results from these experiments has been prepared with high-resolution pedestal measurements; this data, herein termed the "pedestal database", will be used for the balance of this paper.

## III. EMPIRICAL SCALINGS

### A. H-Mode Baselines

To understand the physics of I-mode, it is useful to compare I-mode pedestals to established scalings for baseline H-modes. First, we consider the ELMy H-mode, common among high-performance tokamaks and considered the baseline scenario for ITER operation [2, 3]. Stationary ELMy H-modes are characterized by bursts of transport through the pedestal driven by Edge-Localized Modes (ELMs), providing the necessary relaxation in particle confinement to avoid radiative collapse. ELMy H-mode pedestal structure appears to be limited primarily by edge MHD instabilities, particularly coupling between pressure-driven ballooning modes and current-driven kink/peeling modes [29–31]. The ballooning MHD instability is expressed as an limit on the normalized pressure gradient $\alpha_{MHD}$ in the pedestal for a general toroidal equilibrium [41],

$$\alpha_{MHD} = -\frac{2}{(2\pi)^2}\frac{\partial V}{\partial \psi}\sqrt{\frac{V}{2\pi^2 R}}\mu_0\frac{dp}{d\psi} \tag{2}$$

This is expressed more intuitively for a cylindrical plasma [42] as

$$\alpha_{MHD} = -\frac{2Rq^2}{B_T^2}\nabla p \tag{3}$$

with the $q^2/B_T^2$ factor effectively expressing the scaling as $\alpha_{MHD} \sim \nabla p/B_p^2$. This is reflected in plasma parameters by the scaling $\nabla p_{ped} \sim I_p^2$, as has been observed in ELMy H-mode experiments [33]. More simply, as pedestal width typically varies over a small range for a given operating configuration [43], we may express the ballooning MHD limit as a simple

limit on pedestal pressure normalized to the poloidal field, $\beta_{p,ped}$. To lowest-order approximation, then, for a given configuration of current, field, and shaping, the pedestal pressure $p \sim n_e T_e$ is limited. Altering the density with a change in fueling results in heating or cooling the pedestal to maintain this limited pedestal pressure; alternately, modifying the pedestal via a change in heating power alters the energy transport (increasing the ELM frequency $f_{ELM} \sim P$ for large Type I ELMs [44]) in response to maintain the limit.

Additionally, we may consider an alternate H-mode regime pioneered on C-Mod, the Enhanced $D_\alpha$ (EDA) H-mode [15, 16]. EDA H-mode is a higher-collisionality ($\nu^*_{95} > 1$) regime, characterized by pedestal regulation through a continuous edge fluctuation, the Quasi-Coherent Mode (QCM), rather than bursty ELM transport. EDA pedestals are limited primarily by transport effects, rather than macroscopic edge MHD instability [34] – higher particle confinement causes the pedestal density to lock to a value set by the plasma current, with additional fueling countered by increased density pumpout. Within this density limit, the pedestal temperature (and therefore pressure) respond positively to input heating power [16].

### B. Temperature Pedestal

I-mode is characterized, in part, by its H-mode-like temperature pedestal and energy confinement. A scan of plasma current from from 0.85 to 1.35 MA in a reversed-field, lower-null shape reveals a positive trend of pedestal temperature with plasma current, as shown in Figure 4, with the I-mode pedestal $T_e$ (for this paper, we use pedestal parameters evaluated at the 95% flux surface) meeting or exceeding that found in ELMy H-modes on C-Mod. There is, however, significant spread at any given point in the $I_p$ scan, due to variation in input heating power. Examining a single current slice (Figure 5), we see a strong dependence of the temperature pedestal height on net heating power, $P_{net} = P_{ICRF} + P_{Ohm} - P_{rad} - dW/dt$, normalized to density (effectively, input power per particle). A consistent pattern is observed at other current points, with the suppressed temperature at the highest current point explained by relatively low $P_{net}/n_e$.

This behavior is generally consistent with the behavior observed in H-modes; a comparable sensitivity of the pedestal (in density, temperature, and pressure) to plasma current is observed in ELMy H-modes [33], although the sensitivity of the temperature pedestal is

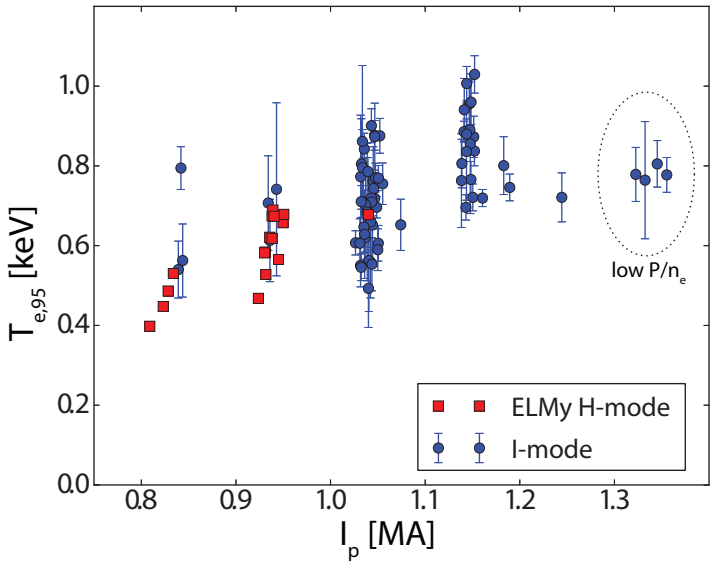


FIG. 4. Pedestal temperature versus plasma current, comparing ELMy H-mode and I-modes. I-mode temperature pedestals meet or exceed H-mode levels, and trend positively with current. The spread at a given current point is due to varying power per particle (see Fig. 5).

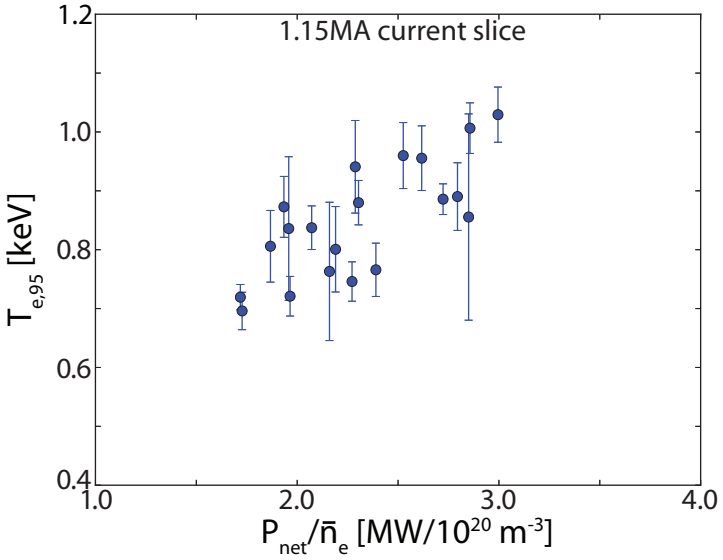


FIG. 5. Pedestal temperature versus heating power per particle, $I_p = 1.15$ MA, illustrating approximate linear trend of pedestal $T_e$ with $P_{net}/\overline{n}_e$ ($P_{net} = P_{ICRF} + P_{Ohm} - P_{rad} - dW/dt$).

weaker than that observed in I-mode. The response of the temperature pedestal to heating power is at least as strong as that observed in transport-limited EDA H-mode pedestals [16], with the sensitivity in EDA H-mode scaling as $T_{e,ped} \propto (P_{net}/\overline{n}_e)^{0.5\pm0.1}$.

### C. Fueling Control and Density Profiles

In contrast to the temperature pedestal (section III B), the edge density in I-mode exhibits markedly different behavior compared to H-mode. Edge density in I-mode is set primarily through operator fueling control via gas puffing, maintaining an L-mode-like density profile without the density pedestal found in H-modes. Given sufficient heating power, temperature pedestals can be maintained alongside increased fueling. Example discharges matched in current, field, and shaping are shown in figure 6, spanning a range in fueling and heating power, $\overline{n}_e = 1.0 - 1.7 \times 10^{20}$ m$^{-3}$, $P_{net} = 2.75 - 4.10$ MW. Temperature pedestals are matched across all three discharges, despite the wide variation in fueling levels and edge densities, using consistent power per particle, $P_{net}/\overline{n}_e = 2.4 - 2.7$ MW/$10^{20}$ m$^{-3}$.

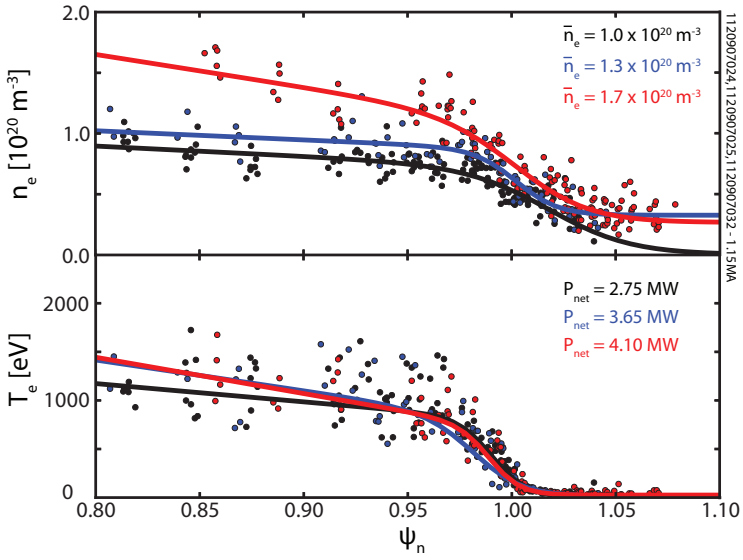


FIG. 6. Three discharges, matched in current (1.1 MA), field (5.6 T) and shaping, fueled to $\overline{n}_e = 1.0, 1.3, 1.7 \times 10^{20}$ m$^{-3}$, spanning a large fraction of the density range in the I-mode discharges presented here. With sufficient heating power (2.75, 3.65, 4.10 MW), temperature pedestals can be matched across the fueling range. This corresponds to power-per-particle values of $P_{net}/\overline{n}_e \sim 2.4 - 2.7$ MW/$10^{20}$ m$^{-3}$.

This behavior is distinct from that found in H-modes on C-Mod – ELMy H-modes at fixed current and shaping exhibit an inverse relationship between pedestal $n_e$ and $T_e$ due to limited pedestal $\beta_p$, while EDA H-mode pedestals lack the fueling control found in I-mode. This is indicative of a path to strongly improved performance in I-mode, increasing pedestal $\beta_p$ and global confinement via matched increases in fueling and heating power, maintaining the target temperature pedestal with appropriate levels of $P_{net}/\overline{n}_e$. Recent experiments on C-Mod [39] have successfully applied this approach, reaching elevated density by fueling into an established I-mode despite the application of heating power levels sufficient for a transition to H-mode at higher starting density.

### D. Pressure Pedestal Scalings

Despite its lack of a density pedestal, I-mode is capable of reaching competitive levels of pedestal thermal pressure, while maintaining favorable behavior in its density and temperature profiles. I-mode pedestal pressure (we use twice the electron pressure measured by Thomson scattering here, consistent with $T_i \approx T_e$ measurements [45]) versus plasma current is depicted in Figure 7, with additional differentiation by fueling level indicated by color. An increase in pedestal pressure at least as $p_{95} \sim I_p$ is observed, consistent with the scaling of the temperature pedestal $T_e \sim I_p$. The pedestal pressure at a given current is seen to increase strongly with increased fueling, consistent with the maintenance of the temperature pedestal with increased heating power alongside increased fueling, maintaining consistent levels of $P_{net}/\overline{n}_e$ (see section III C). The effect of heating power on the pressure pedestal is visible in Figure 8, showing a single current slice from the scan. At fixed current, the pressure pedestal scales as $p_{95} \sim P_{net}$, consistent with the previously observed $T_{e,ped} \sim P_{net}/\overline{n}_e$ trend in the temperature pedestal. This is consistent with the favorable scaling of energy confinement with heating power – plasma stored energy, which is set to lowest order by heating power and energy confinement times $W \sim P\tau_E$, is strongly influenced by pedestal pressure. Thus, the trend $p_{ped} \sim P_{net}$ is consistent with little or no degradation of $\tau_E$ with heating power, which has been observed in global measurements of I-mode [20, 46] (see Figure 9), and is distinct from the $\tau_E \sim P^{-0.7}$ scaling found for ELMy H-modes [2].

Trends in the pressure pedestal in I-mode are also indicative of MHD stability. As shown in Figure 10, the peak pressure gradient (identified as the driver for ballooning MHD

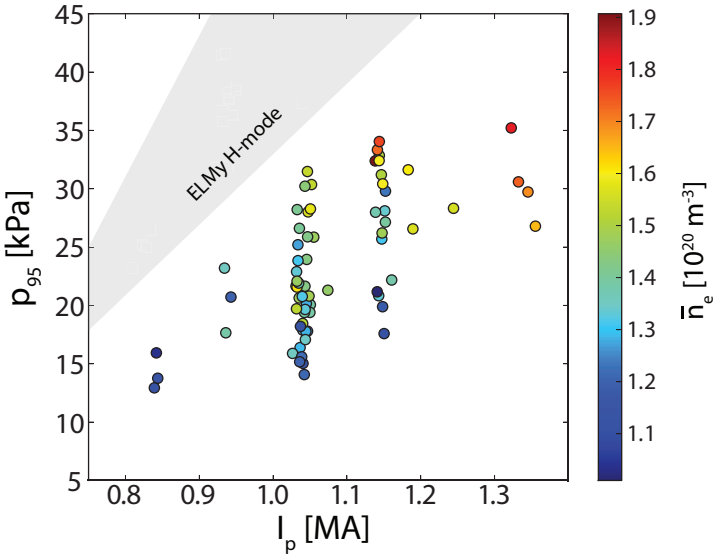


FIG. 7. Pedestal thermal pressure ($2 \times p_{e,95}$) versus plasma current, colored by fueling level. The shaded region indicates the typical range of pedestal pressures in C-Mod ELMy H-modes. A strong, roughly $p_{95} \sim I_p$ trend of pedestal pressure with plasma current is observed. At a given current, a strong increase of pedestal pressure with density is also observed (note: heating power also varied in these discharges).

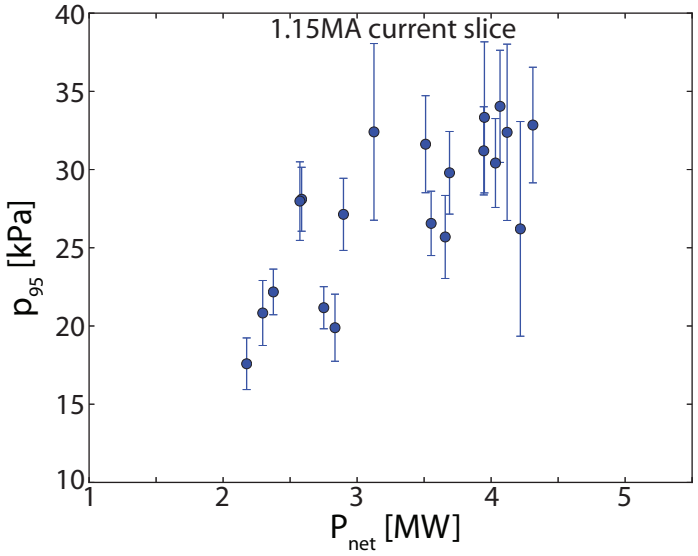


FIG. 8. Pedestal pressure ($2 \times p_{e,95}$) versus net heating power, $I_p = 1.15$ MA, illustrating the trend $p_{95} \sim P_{net}$, consistent with the power trending in I-mode temperature pedestals, $T_{e,95} \sim P_{net}/\overline{n}_e$.

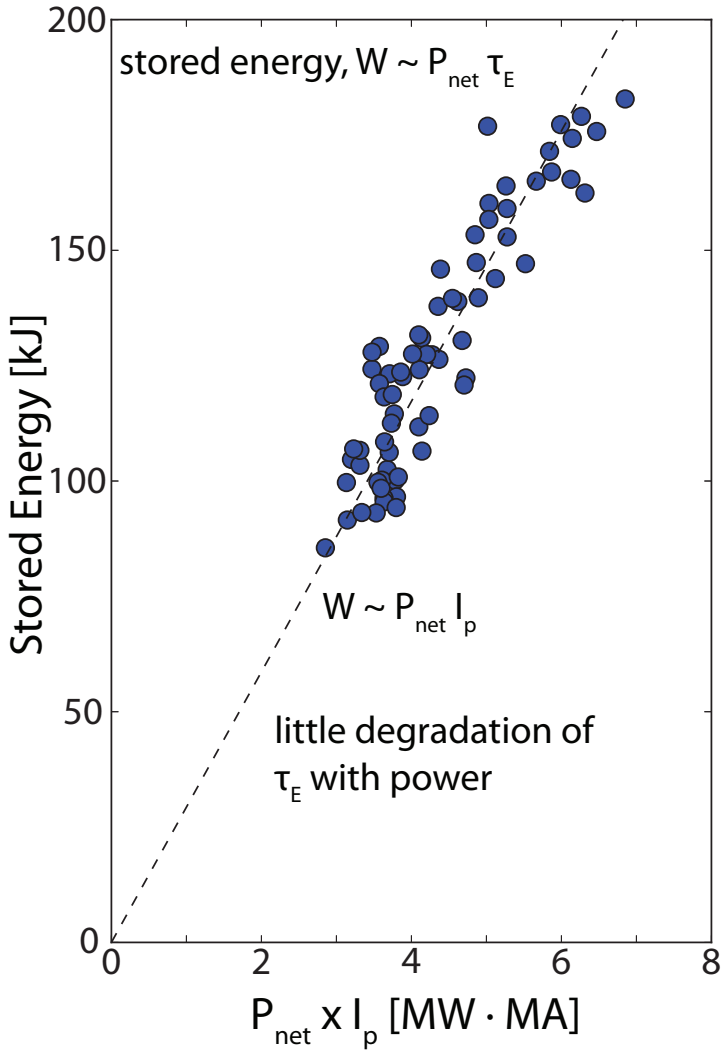


FIG. 9. I-mode stored energy versus the heating power $P_{net}$ times plasma current $I_p$. Stored energy $W$ scales as $P_{net}\tau_E$. From H-mode scalings, energy confinement time $\tau_E$ is expected to scale roughly linearly with current, and to show a strong degradation with heating power: $\tau_E \sim I_p \times P_{net}^{-0.7} \rightarrow W \sim I_p \times P_{net}^{0.3}$. The observed roughly linear relationship, $W \sim I_p \times P_{net}$, indicates little to no degradation of $\tau_E$ with heating power in I-mode.

instabilities) in I-mode is consistently shallower at a given $I_p$ than comparable ELMy H-modes on C-Mod, due to the flat edge density profile. Moreover, pedestal pressure gradient scales more weakly than the expected $\nabla p \sim I_p^2$ expected from the ballooning stability boundary (arising from the critical normalized gradient $\alpha_{MHD}$ identified with ballooning drive [42]). This is consistent with the observed lack of large ELMs in I-mode operation, indicating that I-mode pedestals are strongly stable to an MHD instability identified with

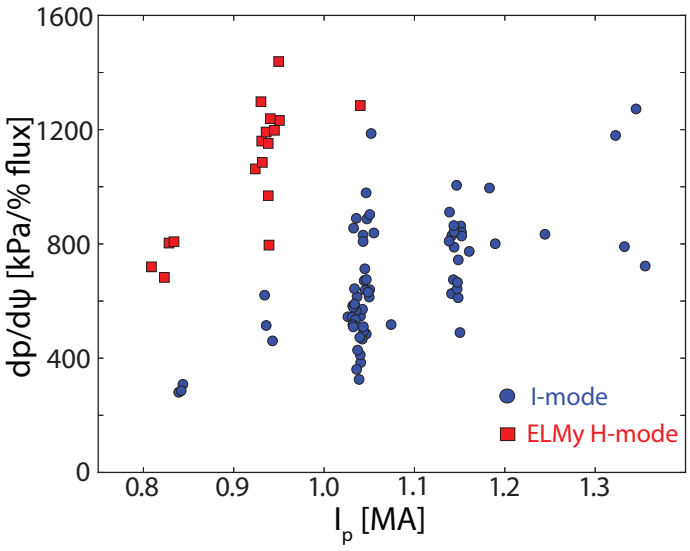


FIG. 10. Peak pressure gradient (measured at pedestal midpoint) versus plasma current for I-mode and ELMy H-mode. I-mode consistently exhibits a weaker pressure gradient, as well as a weaker scaling than $\nabla p \sim I_p^2$ expected from ballooning MHD stability limits.

the ELM trigger.

## IV. MHD MODELING

In addition to its favorable pedestal scalings in terms of performance, I-mode is characterized by consistent stability against large, deleterious Edge-Localized Modes (ELMs). ELM triggering in H-mode has been identified with the interaction between pressure-driven ballooning and current-driven kink/peeling MHD instabilities in the pedestal [29–31]. Detailed numerical studies of the MHD instabilities associated with ELM drive are accomplished through the ELITE code [30, 47]. This method is also used for the MHD stability component of the predictive EPED model [26–28]. MHD stability modeling has been successfully applied on C-Mod in ELMy [33] and EDA [34] H-modes, and in extensive cross-machine H-mode studies [25].

The MHD stability of I-mode pedestals in ELITE (Figure 11) is consistent with the generally observed lack of ELMs – the I-mode pedestal is strongly stable to peeling-ballooning MHD instabilities, as the lack of a strong density pedestal both reduces the total pressure gradient (reducing ballooning drive) and the bootstrap current drive (reducing kink/peeling

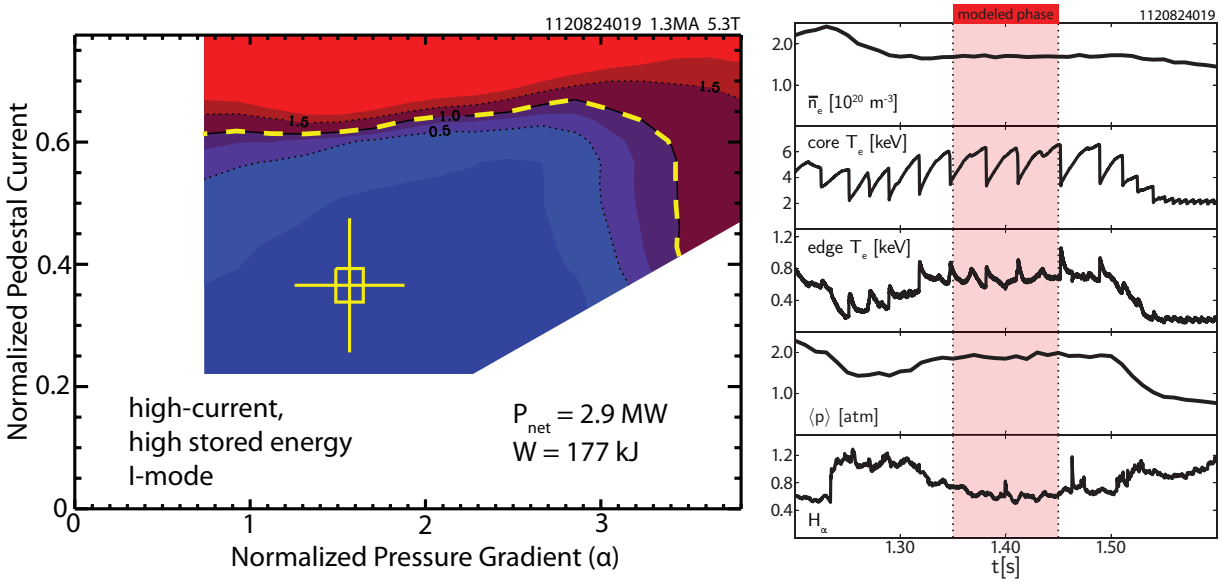


FIG. 11. I-mode pedestal MHD stability contour generated by ELITE. Stability boundary indicated by the yellow dash. Parameters for modeled window shown at right.

drive). However, under certain conditions, particularly reduced toroidal field and plasma current, small ($< 1\%$ drop in stored energy) intermittent ELM-like events are occasionally observed in I-mode. Examining the MHD stability of these cases (Figure 12), we see that these cases are nevertheless far from the peeling-ballooning stability boundary. These intermittent events occur shortly following sawtooth heat pulses reaching the edge, indicating a possible trigger due to transient modification of the pedestal – however, ELM events are not consistently triggered by every heat pulse under similar conditions. Alternately, the events may be indicative of a distinct phenomenon from large ELMs independent of peeling-ballooning MHD instability. More study is required on this front.

Examination of I-mode pedestal parameters is also illuminating from the perspective of MHD stability. Pedestal temperature versus density for I-mode and ELMy H-modes on C-Mod is shown in Figure 13(a). The pedestal parameters shown are normalized to edge poloidal field – this both provides normalization to current, and allows an intuitive picture of ballooning MHD stability, as hyperbolas in the parameter space are curves of constant pedestal poloidal beta. ELMy H-modes in a given shape are observed to lie on the expected $\beta_p$-limited curve, with an inverse relationship between pedestal density and temperature; I-mode pedestal density and temperature, on the other hand, are uncorrelated, consistent with the pedestal not being limited by ballooning MHD instability. Pedestal pressure versus

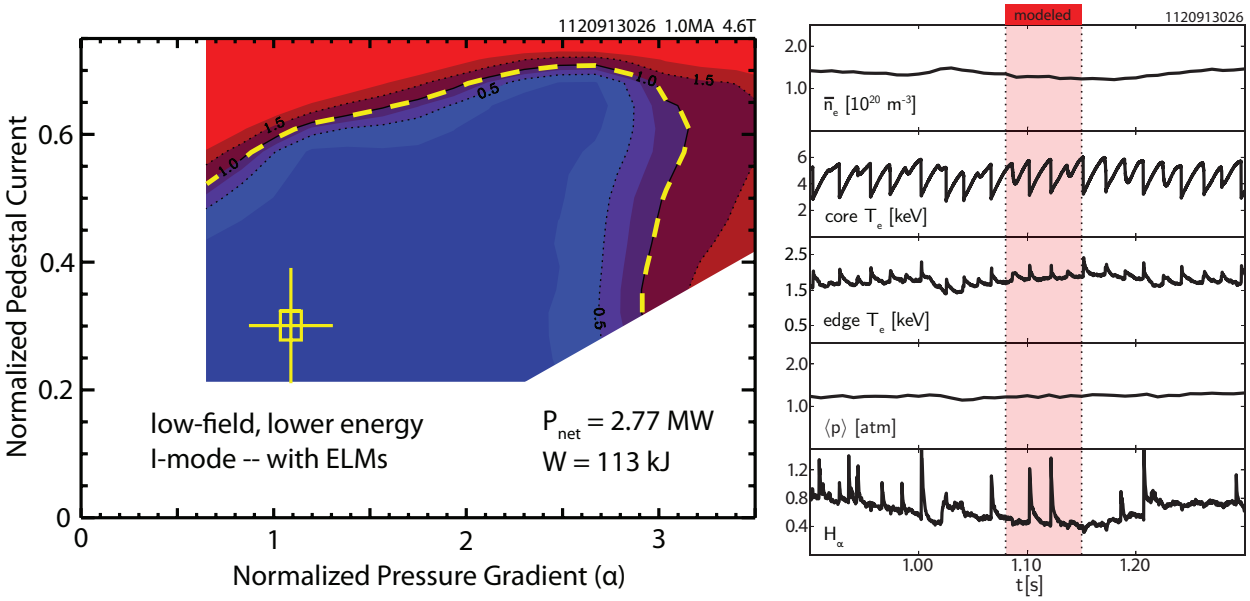


FIG. 12. ELITE stability contour for I-mode featuring small, intermittent ELMs. The pedestal is still stable to conventional MHD ELM triggering. Parameters for modeled window shown at rightp.

density, similarly normalized, is shown in figure 13(b). The linear response of pedestal $\beta_p$ with (normalized) density is consistent with the strong response of the pedestal pressure with fueling observed in figure 7. The constant slope, set by $T_e/B_p$, is consistent with the $T_{e,ped} \sim I_p$ scaling previously observed as well.

## V. KINETIC-BALLOONING TURBULENCE

Edge turbulence in I-mode is characterized by a strong reduction of mid-frequency turbulence and the appearance of a higher-frequency ($\sim 200 - 400$ kHz) fluctuation, dubbed the "weakly-coherent mode" (WCM) [20, 45, 46, 48]. The WCM is well-characterized experimentally, with density, temperature, and magnetic fluctuations visible on multiple diagnostics [46, 48, 49]. However, as the density fluctuation is typically stronger by a factor of 5-10 [48], the mode is treated as predominantly a density fluctuation, consistently measured via reflectometry [46] and gas-puff imaging [48]. The WCM appears to be connected to the density pumpout and pedestal regulation in I-mode, with the WCM amplitude shown to be correlated to particle flux through the LCFS [46]. The underlying physics of the WCM and its regulation of the pedestal, then, is of high importance to the understanding of I-

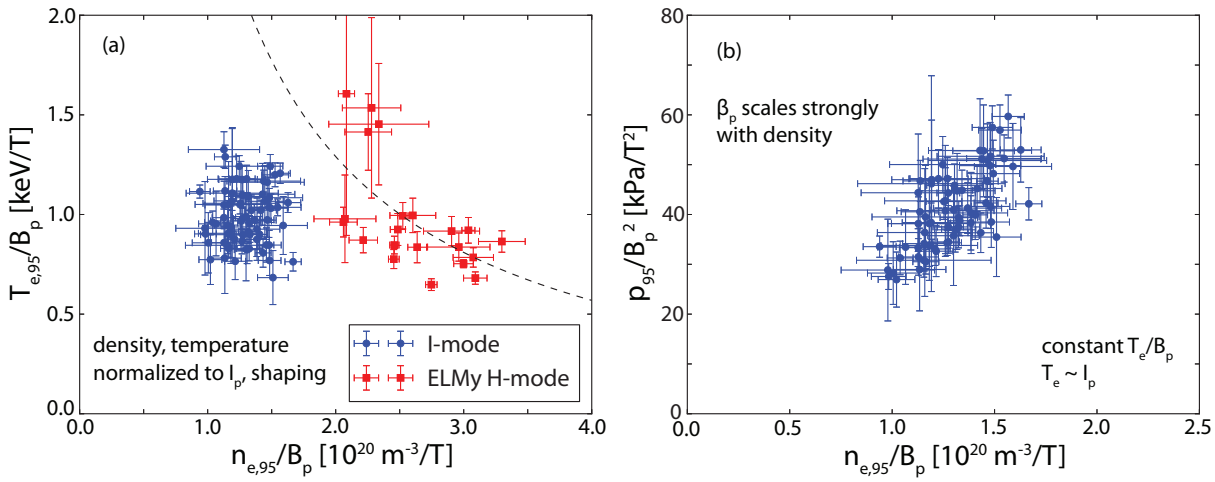


FIG. 13. Pedestal parameters versus pedestal density. Parameters are normalized by edge poloidal field – this provides normalization to current, as well as allowing a natural representation of MHD boundaries. (a) Pedestal temperature vs. density for I-modes and ELMy H-modes. Due to the normalization to edge $B_p$, hyperbolas in the phase space are curves of constant $\beta_{p,ped}$. ELMy H-modes lie on a $\beta_p$-limited curve (indicated by the dashed line), with the expected inverse relationship between pedestal density and temperature; I-mode $n_e$ and $T_e$, however, are uncorrelated. (b) Normalized pedestal pressure vs. density in I-mode. Pedestal $\beta_p$ is linearly dependent on normalized density, rather than lying on a $\beta_p$-limited line (as with ELMy H-mode), consistent with the strong response of I-mode pedestals to increased fueling. I-mode data lie on a line of constant $T_e/B_p$, consistent with the observed $T_{e,ped} \sim I_p$ scaling reported in section III B.

mode. An important starting point from the standpoint of ELM stability and turbulence characterization, then, is the Kinetic Ballooning Mode (KBM) observed in ELMy H-modes.

EPED modeling in ELMy H-modes [26–28] uses KBM turbulence as an additional constraint on the pedestal at the ELM stability boundary – KBM turbulence and peeling-ballooning MHD set distinct constraints on the pressure pedestal width and height ($p_{ped} \sim \Delta_\psi^{3/4}$ from peeling-ballooning MHD, $p_{ped} \sim \Delta_\psi^2$ from KBM turbulence, using the pedestal width in normalized poloidal flux space $\Delta_\psi$), with their intersection setting the predicted pedestal at the ELM crash. ELMy H-mode studies [25] have established a predictive line for KBM-limited pedestals used in EPED, with the width (in normalized poloidal flux) predicted by $\Delta_\psi = 0.076\beta_{p,ped}^{1/2}$. A comparison of I-mode pedestals against this predictive line, as well as C-Mod ELMy H-modes, is shown in figure 14. I-mode pedestals are wider on

average than predicted by the KBM-limited ($\sim \beta_{p,ped}^{1/2}$) line, and show no trend of pedestal width with poloidal beta, consistent with stability against the turbulence identified with the ELM trigger.

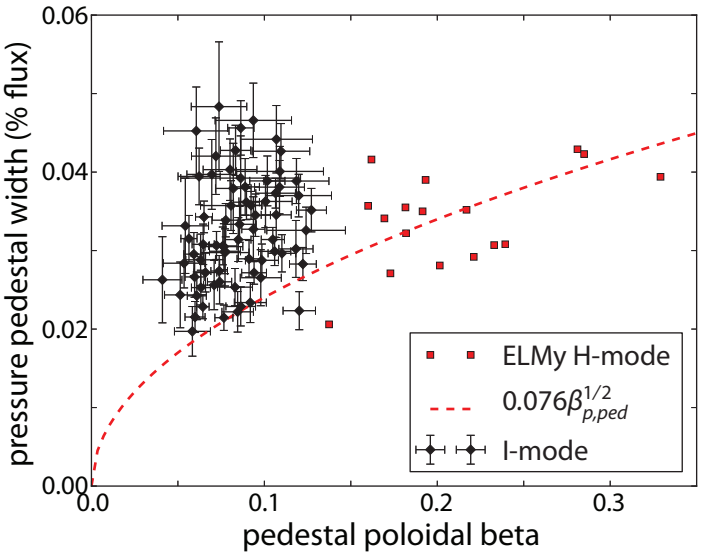


FIG. 14. Pedestal width versus poloidal beta in I-mode and ELMy H-mode. ELMy H-modes lie on the line $\Delta_\psi = 0.076\beta_{p,ped}^{1/2}$ predicted for KBM-limited pedestals. I-mode shows no scaling of pedestal width with $\beta_p$, and exhibit pedestals consistently wider than predicted for ELM-limited pedestals.

Computational modeling of KBM stability is also possible, using infinite-$n$ ballooning MHD stability calculated by BALOO [50] as a surrogate for the turbulence threshold [26, 32]. As infinite-$n$ modes are perfectly localized on rational surfaces, it is not possible to model the pedestal as unstable to a single mode – rather, the "ballooning-critical pedestal" (BCP) technique [27] takes the KBM threshold to be where the pressure gradient is sufficiently high for half of the pedestal width to be ballooning critical (i.e., containing infinite-$n$ unstable surfaces). Infinite-$n$ modeling results for two test cases are shown in figure 15, overlaid on their finite-$n$ ELITE modeling results (see figures 11 and 12). The two cases span the range in pedestal widths of the I-mode cases considered here (see figure 14), with case (a) near the KBM-limited prediction line, $\Delta_{EPED} = 0.076\beta_{p,ped}^{1/2}$, and case (b) far from the predicted line. In both cases, the pedestal is found to be far from the ballooning critical threshold.

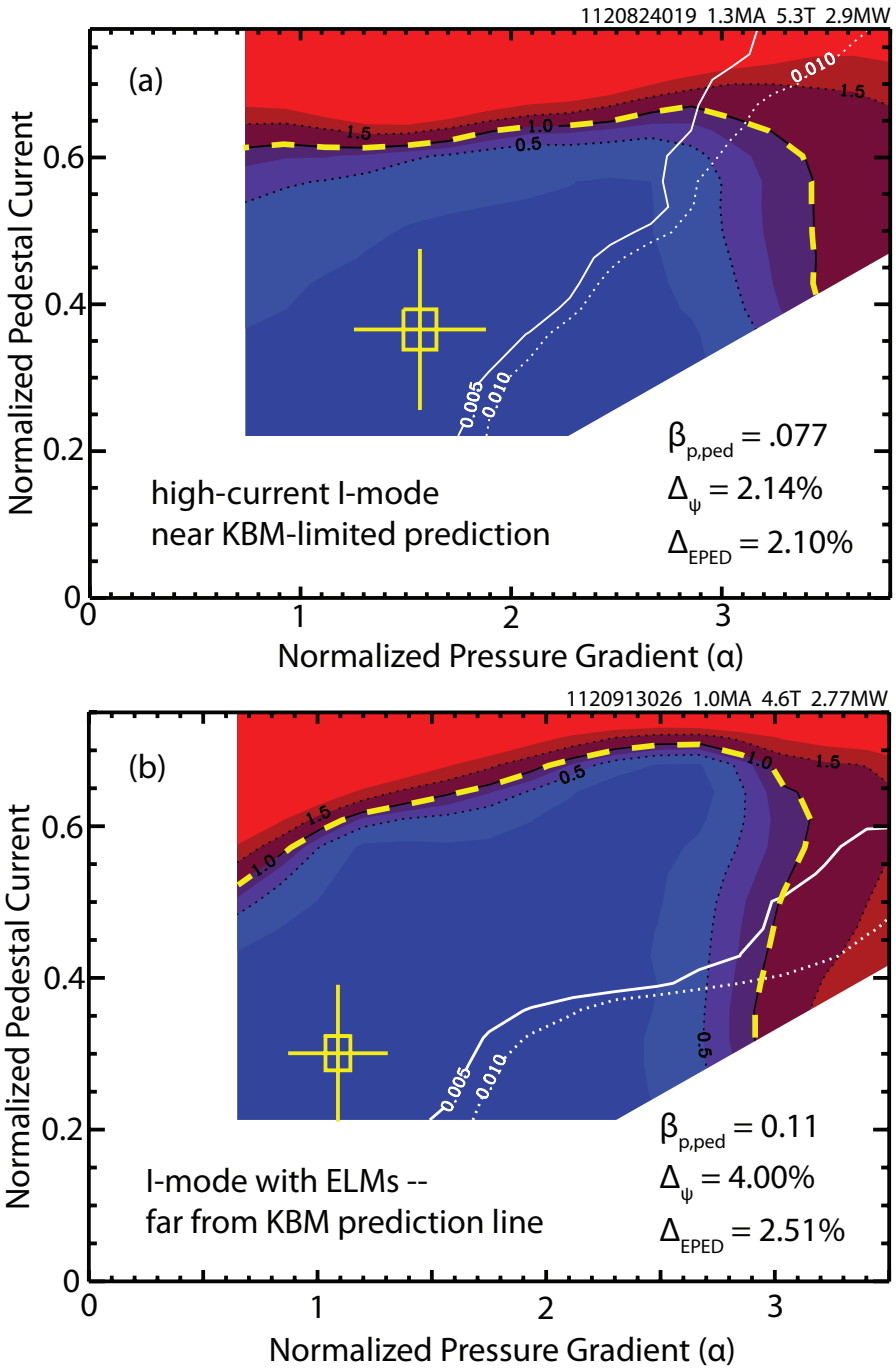


FIG. 15. Infinite-$n$ MHD stability predictions, overlaid on finite-$n$ ELITE calculation (see figures 11 and 12). Contours depict the percentage of poloidal flux covered by infinite-$n$ unstable surfaces; the KBM threshold is set where half of the pedestal is thus unstable. (a) Low pedestal width case, with experimental $\Delta_\psi$ near level predicted by KBM/EPED theory ($\Delta_{EPED} = 0.076\beta_{p,ped}^{1/2}$). (b) High pedestal width case, far from KBM theory prediction. In both cases, the pedestal is not near the BALOO-predicted KBM stability boundary.

## VI. CONCLUSIONS

I-mode is a promising alternate regime for ITER and reactor-scale operation, characterized by its apparent decoupling of energy and particle transport channels. I-mode operation generates a high-temperature, low-collisionality pedestal (with natural operation near ITER target $\nu^*_{95}$ and $q_{95}$, as shown in Figure 2) with comparable energy confinement to more conventional H-modes. At the same time, I-mode lacks a density pedestal or significant reduction in particle transport, maintaining desirable L-mode-like levels of impurity confinement for stationary operation with high-$Z$ metal wall materials. I-mode appears to be naturally free of large ELMs, avoiding the deleterious pulsed heat loading anticipated for uncontrolled ELMy H-modes in ITER-scale devices without the need for externally-applied ELM mitigation or suppression. Additionally, scalings of global stored energy with heating power in I-mode are consistent with little or no degradation of energy confinement with heating power [20], in contrast to ELMy H-mode (approximately $\tau_E \sim P^{-0.7}$ from multi-machine analysis [2]), a potentially highly favorable scaling to reactor-scale devices.

A firm understanding of the pedestal is essential for extrapolation of high-performance regimes to ITER and reactor-scale devices. Mirroring recent successes in theory, modeling, and cross-machine experiment in ELMy H-mode [25, 27], we applied three approaches in the study of I-mode pedestals: empirical scalings of the pedestal with engineering parameters, computational modeling of pedestal stability against peeling-ballooning MHD instabilities, and investigation of the turbulent characteristics constraining the I-mode pedestal.

An empirical examination of the I-mode pedestal (section III) reveals pedestal scalings consistent with other high-performance regimes, modified by the enhanced particle transport in I-mode. The temperature pedestal is found to scale strongly with plasma current and heating power per particle, $T_{e,ped} \sim P_{net}/\overline{n}_e$. The pressure pedestal, likewise, exhibits a scaling $p_{ped} \sim I_p$, comparable to ELMy H-mode on C-Mod [33]. Moreover, the pedestal pressure scales strongly with heating power, $p_{ped} \sim n_e T_e \sim P_{net}$ – a significantly stronger response than in ELMy or EDA H-modes on C-Mod, and consistent with the observed weak degradation of global energy confinement with heating power in I-mode [20, 46].

In contrast to its H-mode-like energy confinement, I-mode exhibits L-mode-like density profiles, with straightforward density control through operator fueling (section III C). Due to the strong response of the temperature pedestal with heating power, and the decoupled

particle and energy transport in I-mode, temperature pedestals can be matched given sufficient heating power across a broad range of fueling levels, in contrast to the trade-off between the $n_e$ and $T_e$ pedestals in ELMy H-mode. This is indicative of a path to increased pedestal $\beta_p$ (and therefore overall performance) – increasing fueling and heating power apace with each other, maintaining an appropriate level of $P_{net}/\overline{n}_e$ to sustain the target temperature pedestal, tuning both the density and temperature profiles to the desired level.

I-mode pedestals are also observed to be strongly stable to the coupled edge peeling and ballooning MHD instabilities identified with the trigger for large, deleterious Type I ELMs [29–31]. I-mode pressure pedestals are observed at a weaker peak pressure gradient than that found in ELMy H-modes, and scale more weakly than the $\nabla p \sim I_p^2$ trend expected from ballooning stability; similarly, the pedestals are not constrained on the $\beta_p$-limited line exhibited by ELMy H-modes. Numerical modeling of peeling-ballooning MHD stability using the ELITE code [30, 47] indicates that I-mode pedestals are far from the computed stability boundary, consistent with the observed lack of large ELMs. However, small, intermittent ELM events have been observed under certain conditions in I-mode. These cases are found to also be peeling-ballooning stable, potentially indicating that these events are distinct phenomena consistent with the observed stability against traditional Type I ELMs in I-mode.

Edge turbulence in I-mode, particularly the mid-frequency "weakly-coherent mode" (WCM) is well-characterized experimentally, but nevertheless the underlying physics basis is poorly understood. I-mode pedestal data are compared to predictions based on kinetic-ballooning mode (KBM) turbulence (section V), which is thought to set a strong constraint on the pedestal in ELMy H-modes [26–28]. I-mode pedestal widths are observed to have no trend with $\beta_{p,ped}$, in contrast to the $\Delta_\psi \propto \beta_{p,ped}^{1/2}$ scaling predicted from KBM physics, and are generally wider than predicted based on KBM-limited physics. Numerical modeling of the KBM threshold using infinite-$n$ ballooning MHD as a surrogate [26, 32] indicates that I-mode pedestals are not limited by kinetic-ballooning turbulence.

Substantial physics work remains in characterizing I-mode pedestals, particularly in understanding the underlying physics of the WCM, expansion of pedestal stability modeling to include additional effects, e.g., resistivity, via additional codes, such as BOUT++ [51], and characterization of the small, intermittent ELM events observed at reduced magnetic field. Nevertheless, observed pedestal phenomena in I-mode are consistent with scalings of

pedestal parameters and confinement competitive with other high-performance regimes, and stability against conventional triggers for large, deleterious ELMs. Further development of I-mode as a candidate reactor regime is ongoing, particularly towards an expansion of the I-mode operating window through improved understanding of I-H threshold physics, and achievement of I-mode operation on other devices.

## ACKNOWLEDGMENTS

Experimental work on Alcator C-Mod is supported by US DOE agreement DE-FC02-99ER54512. Theory work at General Atomics is supported by US DOE agreement DE-FG02-99ER54309. The authors also wish to acknowledge the efforts of the Alcator C-Mod group for supporting the experiments reported here.

---

[1] F. Wagner, G. Becker, K. Behringer, D. Campbell, A. Eberhagen, W. Engelhardt, G. Fussmann, O. Gehre, J. Gernhardt, G. v. Gierke, G. Haas, M. Huang, F. Karger, M. Keilhacker, O. Klüber, M. Kornherr, K. Lackner, G. Lisitano, G. G. Lister, H. M. Mayer, D. Meisel, E. R. Müller, H. Murmann, H. Niedermeyer, W. Poschenrieder, H. Rapp, H. Röhr, F. Schneider, G. Siller, E. Speth, A. Stäbler, K. H. Steuer, G. Venus, O. Vollmer, and Z. Yü, Phys. Rev. Lett. **49**, 1408 (1982).

[2] ITER Physics Expert Group on Confinement, Transport and ITER Physics Expert Group on Confinement Modelling and Database, and ITER Physics Basis Editors, Nuclear Fusion **39**, 2175 (1999).

[3] M. Shimada, D. Campbell, V. Mukhovatov, M. Fujiwara, N. Kirneva, K. Lackner, M. Nagami, V. Pustovitov, N. Uckan, J. Wesley, N. Asakura, A. Costley, A. Donn, E. Doyle, A. Fasoli, C. Gormezano, Y. Gribov, O. Gruber, T. Hender, W. Houlberg, S. Ide, Y. Kamada, A. Leonard, B. Lipschultz, A. Loarte, K. Miyamoto, V. Mukhovatov, T. Osborne, A. Polevoi, and A. Sips, Nuclear Fusion **47**, S1 (2007).

[4] J. Kinsey, G. Staebler, J. Candy, R. Waltz, and R. Budny, Nuclear Fusion **51**, 083001 (2011).

[5] G. T. A. Huysmans, Plasma Physics and Controlled Fusion **47**, B165 (2005).

[6] P. Maget, J.-F. Artaud, M. Bcoulet, T. Casper, J. Faustin, J. Garcia, G. Huijsmans, A. Loarte,

and G. Saibene, Nuclear Fusion **53**, 093011 (2013).

[7] P. B. Snyder, H. R. Wilson, J. R. Ferron, L. L. Lao, A. W. Leonard, T. H. Osborne, A. D. Turnbull, D. Mossessian, M. Murakami, and X. Q. Xu, Physics of Plasmas **9**, 2037 (2002).

[8] A. Loarte, G. Saibene, R. Sartori, D. Campbell, M. Becoulet, L. Horton, T. Eich, A. Herrmann, G. Matthews, N. Asakura, A. Chankin, A. Leonard, G. Porter, G. Federici, G. Janeschitz, M. Shimada, and M. Sugihara, Plasma Physics and Controlled Fusion **45**, 1549 (2003).

[9] G. Federici, A. Loarte, and G. Strohmayer, Plasma Physics and Controlled Fusion **45**, 1523 (2003).

[10] L. R. Baylor, N. Commaux, T. C. Jernigan, S. J. Meitner, S. K. Combs, R. C. Isler, E. A. Unterberg, N. H. Brooks, T. E. Evans, A. W. Leonard, T. H. Osborne, P. B. Parks, P. B. Snyder, E. J. Strait, M. E. Fenstermacher, C. J. Lasnier, R. A. Moyer, A. Loarte, G. T. A. Huijsmans, and S. Futatani, Physics of Plasmas **20**, 082513 (2013).

[11] T. E. Evans, R. A. Moyer, P. R. Thomas, J. G. Watkins, T. H. Osborne, J. A. Boedo, E. J. Doyle, M. E. Fenstermacher, K. H. Finken, R. J. Groebner, M. Groth, J. H. Harris, R. J. La Haye, C. J. Lasnier, S. Masuzaki, N. Ohyabu, D. G. Pretty, T. L. Rhodes, H. Reimerdes, D. L. Rudakov, M. J. Schaffer, G. Wang, and L. Zeng, Phys. Rev. Lett. **92**, 235003 (2004).

[12] O. Schmitz, T. Evans, M. Fenstermacher, M. Lehnen, H. Stoschus, E. Unterberg, J. Coenen, H. Frerichs, M. Jakubowski, R. Laengner, C. Lasnier, S. Mordijck, R. Moyer, T. Osborne, H. Reimerdes, D. Reiter, U. Samm, B. Unterberg, the DIII-D, and T. teams, Nuclear Fusion **52**, 043005 (2012).

[13] R. A. Moyer, T. E. Evans, T. H. Osborne, P. R. Thomas, M. Becoulet, J. Harris, K.-H. Finken, J. A. Boedo, E. J. Doyle, M. E. Fenstermacher, P. Gohil, R. J. Groebner, M. Groth, G. L. Jackson, R. J. La Haye, C. J. Lasnier, A. W. Leonard, G. R. McKee, H. Reimerdes, T. L. Rhodes, D. L. Rudakov, M. J. Schaffer, P. B. Snyder, M. R. Wade, G. Wang, J. G. Watkins, W. P. West, and L. Zeng, Physics of Plasmas (1994-present) **12**, 056119 (2005).

[14] A. Kirk, I. T. Chapman, J. Harrison, Y. Liu, E. Nardon, S. Saarelma, R. Scannell, A. J. Thornton, and the MAST team, Plasma Physics and Controlled Fusion **55**, 015006 (2013).

[15] M. Greenwald, N. Basse, P. Bonoli, R. Bravenec, E. Edlund, D. Ernst, C. Fiore, R. Granetz, A. Hubbard, J. Hughes, I. Hutchinson, J. Irby, B. LaBombard, L. Lin, Y. Lin, B. Lipschultz, E. Marmar, D. Mikkelsen, D. Mossessian, P. Phillips, M. Porkolab, J. Rice, W. Rowan, S. Scott, J. Snipes, J. Terry, S. Wolfe, S. Wukitch, and K. Zhurovich, Fusion Science and

Technology **51**, 266 (2007).

[16] A. E. Hubbard, R. L. Boivin, R. S. Granetz, M. Greenwald, J. W. Hughes, I. H. Hutchinson, J. Irby, B. LaBombard, Y. Lin, E. S. Marmar, A. Mazurenko, D. Mossessian, E. Nelson-Melby, M. Porkolab, J. A. Snipes, J. Terry, S. Wolfe, S. Wukitch, B. A. Carreras, V. Klein, and T. S. Pedersen, Physics of Plasmas (1994-present) **8**, 2033 (2001).

[17] K. H. Burrell, M. E. Austin, D. P. Brennan, J. C. DeBoo, E. J. Doyle, P. Gohil, C. M. Greenfield, R. J. Groebner, L. L. Lao, T. C. Luce, M. A. Makowski, G. R. McKee, R. A. Moyer, T. H. Osborne, M. Porkolab, T. L. Rhodes, J. C. Rost, M. J. Schaffer, B. W. Stallard, E. J. Strait, M. R. Wade, G. Wang, J. G. Watkins, W. P. West, and L. Zeng, Plasma Physics and Controlled Fusion **44**, A253 (2002).

[18] A. Garofalo, W. Solomon, J.-K. Park, K. Burrell, J. DeBoo, M. Lanctot, G. McKee, H. Reimerdes, L. Schmitz, M. Schaffer, and P. Snyder, Nuclear Fusion **51**, 083018 (2011).

[19] P. B. Snyder, T. H. Osborne, K. H. Burrell, R. J. Groebner, A. W. Leonard, R. Nazikian, D. M. Orlov, O. Schmitz, M. R. Wade, and H. R. Wilson, Physics of Plasmas (1994-present) **19**, 056115 (2012).

[20] D. Whyte, A. Hubbard, J. Hughes, B. Lipschultz, J. Rice, E. Marmar, M. Greenwald, I. Cziegler, A. Dominguez, T. Golfinopoulos, N. Howard, L. Lin, R. McDermott, M. Porkolab, M. Reinke, J. Terry, N. Tsujii, S. Wolfe, S. Wukitch, Y. Lin, and the Alcator C-Mod Team, Nuclear Fusion **50**, 105005 (2010).

[21] R. M. McDermott, *Edge radial electric field studies via charge exchange recombination spectroscopy on the Alcator C-Mod tokamak*, Ph.D. thesis, Massachusetts Institute of Technology (2009).

[22] I. H. Hutchinson, R. Boivin, F. Bombarda, P. Bonoli, S. Fairfax, C. Fiore, J. Goetz, S. Golovato, R. Granetz, M. Greenwald, S. Horne, A. Hubbard, J. Irby, B. LaBombard, B. Lipschultz, E. Marmar, G. McCracken, M. Porkolab, J. Rice, J. Snipes, Y. Takase, J. Terry, S. Wolfe, C. Christensen, D. Garnier, M. Graf, T. Hsu, T. Luke, M. May, A. Niemczewski, G. Tinios, J. Schachter, and J. Urbahn, Physics of Plasmas **1**, 1511 (1994).

[23] R. M. McDermott, B. Lipschultz, J. W. Hughes, P. J. Catto, A. E. Hubbard, I. H. Hutchinson, R. S. Granetz, M. Greenwald, B. LaBombard, K. Marr, M. L. Reinke, J. E. Rice, D. Whyte, and A. C.-M. Team, Physics of Plasmas **16**, 056103 (2009).

[24] C. Theiler, R. Churchill, B. Lipschultz, T. Puetterich, A. Diallo, A. Hubbard, J. Hughes,

E. Marmar, M. Reinke, J. Terry, J. Walk, and D. Whyte, in *54th Meeting of the APS Division of Plasma Physics* (2012).

[25] R. Groebner, C. Chang, J. Hughes, R. Maingi, P. Snyder, X. Xu, J. Boedo, D. Boyle, J. Callen, J. Canik, I. Cziegler, E. Davis, A. Diallo, P. Diamond, J. Elder, D. Eldon, D. Ernst, D. Fulton, M. Landreman, A. Leonard, J. Lore, T. Osborne, A. Pankin, S. Parker, T. Rhodes, S. Smith, A. Sontag, W. Stacey, J. Walk, W. Wan, E.-J. Wang, J. Watkins, A. White, D. Whyte, Z. Yan, E. Belli, B. Bray, J. Candy, R. Churchill, T. Deterly, E. Doyle, M. Fenstermacher, N. Ferraro, A. Hubbard, I. Joseph, J. Kinsey, B. LaBombard, C. Lasnier, Z. Lin, B. Lipschultz, C. Liu, Y. Ma, G. McKee, D. Ponce, J. Rost, L. Schmitz, G. Staebler, L. Sugiyama, J. Terry, M. Umansky, R. Waltz, S. Wolfe, L. Zeng, and S. Zweben, Nuclear Fusion **53**, 093024 (2013).

[26] P. B. Snyder, R. J. Groebner, A. W. Leonard, T. H. Osborne, and H. R. Wilson, Physics of Plasmas **16**, 056118 (2009).

[27] P. Snyder, R. Groebner, J. Hughes, T. Osborne, M. Beurskens, A. Leonard, H. Wilson, and X. Xu, Nuclear Fusion **51**, 103016 (2011).

[28] P. Snyder, N. Aiba, M. Beurskens, R. Groebner, L. Horton, A. Hubbard, J. Hughes, G. Huysmans, Y. Kamada, A. Kirk, C. Konz, A. Leonard, J. Lnnroth, C. Maggi, R. Maingi, T. Osborne, N. Oyama, A. Pankin, S. Saarelma, G. Saibene, J. Terry, H. Urano, and H. Wilson, Nuclear Fusion **49**, 085035 (2009).

[29] P. Snyder, H. Wilson, J. Ferron, L. Lao, A. Leonard, D. Mossessian, M. Murakami, T. Osborne, A. Turnbull, and X. Xu, Nuclear Fusion **44**, 320 (2004).

[30] H. R. Wilson, P. B. Snyder, G. T. A. Huysmans, and R. L. Miller, Physics of Plasmas **9**, 1277 (2002).

[31] H. R. Wilson, S. C. Cowley, A. Kirk, and P. B. Snyder, Plasma Physics and Controlled Fusion **48**, A71 (2006).

[32] P. B. Snyder and G. W. Hammett, Physics of Plasmas **8**, 744 (2001).

[33] J. Walk, P. Snyder, J. Hughes, J. Terry, A. Hubbard, and P. Phillips, Nuclear Fusion **52**, 063011 (2012).

[34] J. Hughes, P. Snyder, J. Walk, E. Davis, A. Diallo, B. LaBombard, S. Baek, R. Churchill, M. Greenwald, R. Groebner, A. Hubbard, B. Lipschultz, E. Marmar, T. Osborne, M. Reinke, J. Rice, C. Theiler, J. Terry, A. White, D. Whyte, S. Wolfe, and X. Xu, Nuclear Fusion **53**, 043016 (2013).

[35] A. Loarte, B. Lipschultz, A. Kukushkin, G. Matthews, P. Stangeby, N. Asakura, G. Counsell, G. Federici, A. Kallenbach, K. Krieger, A. Mahdavi, V. Philipps, D. Reiter, J. Roth, J. Strachan, D. Whyte, R. Doerner, T. Eich, W. Fundamenski, A. Herrmann, M. Fenstermacher, P. Ghendrih, M. Groth, A. Kirschner, S. Konoshima, B. LaBombard, P. Lang, A. Leonard, P. Monier-Garbet, R. Neu, H. Pacher, B. Pegourie, R. Pitts, S. Takamura, J. Terry, E. Tsitrone, the ITPA Scrape-off Layer, and D. P. T. Group, Nuclear Fusion **47**, S203 (2007).

[36] J. L. Terry, B. LaBombard, B. Lipschultz, M. J. Greenwald, J. E. Rice, and S. J. Zweben, Fusion Science and Technology **51**, 342 (2007).

[37] B. LaBombard, J. L. Terry, J. W. Hughes, D. Brunner, J. Payne, M. L. Reinke, I. Cziegler, R. Granetz, M. Greenwald, I. H. Hutchinson, J. Irby, Y. Lin, B. Lipschultz, Y. Ma, E. S. Marmar, W. L. Rowan, N. Tsujii, G. Wallace, D. G. Whyte, S. Wolfe, S. Wukitch, G. Wurden, and A. C.-M. Team, Physics of Plasmas **18**, 056104 (2011).

[38] A. Hubbard, D. Whyte, R. Churchill, A. Dominguez, J. Hughes, Y. Ma, E. Marmar, Y. Lin, M. Reinke, and A. White, Nuclear Fusion **52**, 114009 (2012).

[39] A. Hubbard, E. Marmar, S. Baek, I. Cziegler, A. Dominguez, M. Greenwald, N. Howard, J. Hughes, B. LaBombard, Y. Lin, B. Lipschultz, M. Reinke, J. Rice, P. Snyder, D. Terry, C. Theiler, A. White, J. Walk, D. Whyte, S. Wukitch, and the Alcator C-Mod Group, in *24th IAEA Fusion Energy Conference*, EX/1-3 (2012).

[40] A. E. Hubbard, J. W. Hughes, I. O. Bespamyatnov, T. Biewer, I. Cziegler, B. LaBombard, Y. Lin, R. McDermott, J. E. Rice, W. L. Rowan, J. A. Snipes, J. L. Terry, S. M. Wolfe, and S. W. A. C.-M. Group (Alcator C-Mod Group), Physics of Plasmas **14**, 056109 (2007).

[41] R. L. Miller, M. S. Chu, J. M. Greene, Y. R. Lin-Liu, and R. E. Waltz, Physics of Plasmas **5**, 973 (1998).

[42] J. W. Connor, R. J. Hastie, and J. B. Taylor, Phys. Rev. Lett. **40**, 396 (1978).

[43] C. Maggi, Nuclear Fusion **50**, 066001 (2010).

[44] H. Urano, W. Suttrop, L. D. Horton, A. Herrmann, J. C. Fuchs, and A. U. Team, Plasma Physics and Controlled Fusion **45**, 1571 (2003).

[45] A. E. Hubbard, D. G. Whyte, R. M. Churchill, I. Cziegler, A. Dominguez, T. Golfinopoulos, J. W. Hughes, J. E. Rice, I. Bespamyatnov, M. J. Greenwald, N. Howard, B. Lipschultz, E. S. Marmar, M. L. Reinke, W. L. Rowan, and J. L. T. A. C.-M. Group (Alcator C-Mod Group),

Physics of Plasmas **18**, 056115 (2011).

[46] A. Dominguez, *Study of Density Fluctuations and Particle Transport at the Edge of I-Mode Plasmas*, Ph.D. thesis, Massachusetts Institute of Technology (2012).

[47] P. B. Snyder and H. R. Wilson, Plasma Physics and Controlled Fusion **45**, 1671 (2003).

[48] I. Cziegler, P. H. Diamond, N. Fedorczak, P. Manz, G. R. Tynan, M. Xu, R. M. Churchill, A. E. Hubbard, B. Lipschultz, J. M. Sierchio, J. L. Terry, and C. Theiler, Physics of Plasmas (1994-present) **20**, 055904 (2013).

[49] A. White, P. Phillips, D. Whyte, A. Hubbard, C. Sung, J. Hughes, A. Dominguez, J. Terry, and I. Cziegler, Nuclear Fusion **51**, 113005 (2011).

[50] J. W. Connor, R. J. Hastie, and J. B. Taylor, Proceedings of the Royal Society of London. A. Mathematical and Physical Sciences **365**, 1 (1979).

[51] T. Xia, X. Xu, and P. Xi, Nuclear Fusion **53**, 073009 (2013).